Energy loss and straggling of MeV Si ions in gases

C. Vockenhuber[a,*], K. Arstila[b], J. Jensen[c], J. Julin[b], H. Kettunen[b], M. Laitinen[b], M. Rossi[b], T. Sajavaara[b], M. Thöni[a], H. J. Whitlow[d,1]

[a]*Laboratory of Ion Beam Physics, ETH Zurich, Otto-Stern-Weg 5, 8093 Zurich, Switzerland*
[b]*Department of Physics, University of Jyväskylä, 40014 Jyväskylä, Finland*
[c]*Department of Physics, Chemistry and Biology, Linköping University, 581 83 Linköping, Sweden*
[d]*Institut des Microtechnologies Appliquées Arc, Haute Ecole Arc Ingénierie, 2300 La Chaux-de-Fonds, Switzerland*

Abstract

We present measurements of energy loss and straggling of Si ions in gases. An energy range from 0.5 to 12 MeV/u was covered using the 6 MV EN tandem accelerator at ETH Zurich, Switzerland, and the K130 cyclotron accelerator facility at the University of Jyväskylä, Finland. Our energy-loss data compare well with calculation based on the SRIM and PASS code. The new straggling measurements support a pronounced peak in He gas at around 4 MeV/u predicted by recent theoretical calculations. The straggling curve structure in the other gases (N_2, Ne, Ar, Kr) is relatively flat in the covered energy range. Although there is a general agreement between the straggling data and the theoretical calculations, the experimental uncertainties are too large to confirm or exclude the predicted weak multi-peak structure in the energy-loss straggling.

Keywords: Energy loss, energy-loss straggling, charge exchange

1. Introduction

Swift heavy ions that penetrate through matter experience both energy loss and energy-loss straggling. The electronic energy-loss straggling of heavy ions is well known to show pronounced deviations from Bohr straggling [1]

$$\Omega^2_{\mathrm{Bohr}} = 4\pi Z_1^2 Z_2 e^4 Nx, \tag{1}$$

where Z_1 and Z_2 are atomic numbers of ion and target, respectively, and Nx is the number of atoms per unit target area.

However, little is known about the systematics of these deviations. One reason being the very scarce amount of available experimental data for energy-loss straggling of heavy ions in various targets [2]. Systematic effects, such as target inhomogeneities, incident-beam energy spread and finite energy resolution also often affect existing measurements, which can lead to erroneous results. This situation is far from satisfying for applications in need of relevant energy-loss straggling data, e.g. ion beam analysis or ion beam therapy, but also makes comparisons with theoretical predictions difficult.

Sigmund et al. [3, 4, 5, 6, 7] have recently made significant progress in understanding the different important contributions to heavy-ion straggling as a function of energy. Theoretically linear straggling (as a result of the interaction with independent target electrons) and non-linear straggling (including bunching of electrons in atoms, packing of atoms in molecules, crystals etc. in addition to charge-exchange straggling in the mean energy loss) contribute to the broadened energy-loss spectrum of the ions [6]. Of these effects charge-exchange straggling can lead in special cases to a strong enhancement over the Bohr straggling. These theoretical considerations indicate even a more complex structure in the energy dependence of heavy-ion straggling, with the possibility of multiple peaks [5]. The progress in the theoretical understanding of straggling yields reliable predictions that can be compared with the frequently adopted semi-empirical model of Yang et al. [8].

In order to provide more reliable experimental data for comparison with theory, we performed energy-loss straggling measurements using different ion beams (Si and Kr), energies and gas targets (He, N_2, Ar, Ne and Kr), which were selected by the guidance of dedicated theoretical calculations [5]. The measurements with Kr beam have been published previously [9] with a reanalysis in [5]. We report here on the measurements with ^{28}Si beam in the energy range 0.5 – 12 MeV/u[2] performed at two accelerator facilities. We describe the experimental setups, the measured data and analysis, and make finally comparisons with semi-empirical result by Yang et al. [8] in addition to recent calculations by Sigmund et al. [5]. Additionally stopping cross sections for Si in the above-mentioned gases are presented.

2. Experimental

In order to cover a large energy range from 0.5 to 12 MeV/u we performed straggling measurements with ^{28}Si beams at two

*corresponding author
Email address: vockenhuber@phys.ethz.ch (C. Vockenhuber)
[1]Present address: Louisiana Accelerator Center, Department of Physics, University of Louisiana at Lafayette, P.O. Box 43680, Louisiana LA 70504, USA.

[2]The unit MeV/u denotes the energy per atomic mass number.

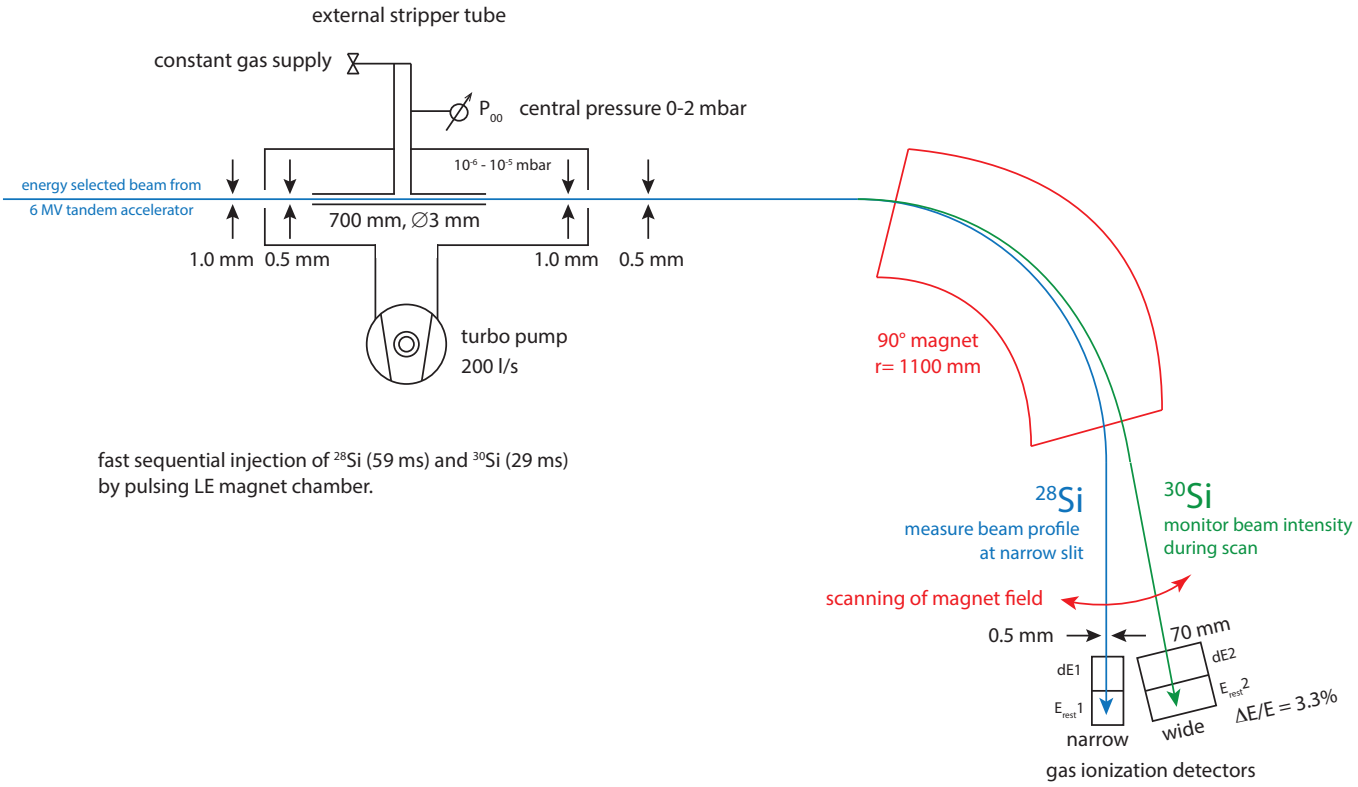

Figure 1: Experimental setup at 6 MV Tandem accelerator at ETH Zurich.

different accelerator facilities using independent measurement techniques: beam energies in the range 0.5 – 2 MeV/u were covered at the 6 MV EN Tandem accelerator at ETH Zurich, Switzerland, and 1 – 12 MeV/u at the K130 cyclotron of the Accelerator Laboratory at the University in Jyväskylä, Finland (JYFL). At ETH Zurich we used an open external gas stripper tube as a windowless gas target followed by energy profile measurement based on a magnetic spectrometer; at JYFL we used time-of-flight (TOF) detectors to determine the energy profile after a gas cell having thin silicon nitride entrance and exit windows. The overlap of measurements at around 1 – 2 MeV/u allowed us to check for any systematic effects that might bias the results at either location. These two setups shall be described in the following sections.

2.1. 6 MV EN tandem accelerator at ETH Zurich

The 6 MV EN tandem accelerator at ETH Zurich can provide Si beams of a wide range of energies up to approximately 2 MeV/u depending on the terminal voltage and the selected charge state. An external stripper canal served as a windowless gas target that can be filled with various gases (Fig. 1). It is located after the charge (and energy) selecting electrostatic analyzer (ESA) and close to the object point of the analyzing magnet. To reach a sufficient target thickness, a 70 cm long tube with a diameter of 3 mm was placed inside the existing stripper canal. The gas is supplied at the middle of tube resulting in a triangular pressure profile. This way, a pressure of up to ~ 2 mbar could be achieved in the middle of the tube without tripping the turbo pumps used for differential pumping. A series of small apertures (0.5 mm and 1 mm diameters) in front and after the stripper reduced contributions from ions scattered on the long tube walls.

The energy-loss profile of the ^{28}Si ions after passing through the gas was determined by scanning the beam using the analyzing magnet with a radius of 1.1 m over a 0.5 mm slit at the image point. The ions were finally counted in a multi-anode gas ionization detector (GID) that allows the clear identification of the Si ions from possible background ions that might reach the detector. Additionally ^{30}Si of same energy was periodically injected using the fast sequencing system at the low-energy magnet. Because of the higher mass ^{30}Si is deflected less in the analyzing magnet and can be measured in a wide GID with an opening of of 70 mm so that an energy range of $\Delta E/E = 3.3\%$ can be accepted, which is wide enough for all measured gas pressures. The measurement times of 59 ms for ^{28}Si and 29 ms for ^{30}Si were adjusted to have approximately equal count rates in both detectors, based on the natural isotopic ratio, the losses through the narrow slits and the broadening of the beam. This procedure allowed us to monitor the primary beam intensity during the scan and thus measure the beam energy profile independent of intensity changes from the ion source (Fig. 2). Additionally, deadtime of the detection system had to be considered as it depends on the actual count rate. Because the count rate of the ^{28}Si changes by 2 – 4 orders of magnitude during the scan over the peak, deadtime is higher at

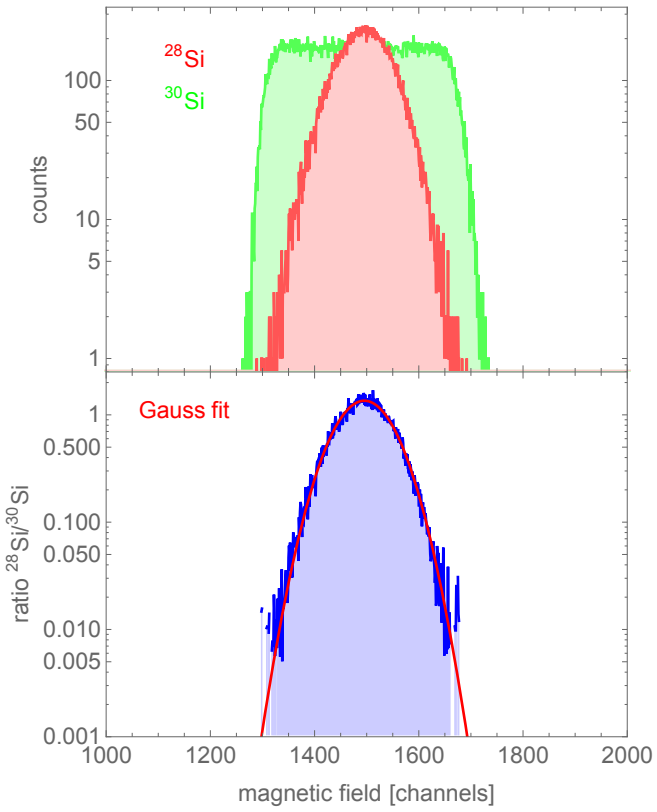

Figure 2: Example of a simultaneous scan of ^{28}Si (top panel, red) over narrow slits and ^{30}Si (top panel, green) measured in the wide detector to monitor beam intensity (0.51 MeV/u, 1.08 mbar Ar, ETH Zurich). The ratio of this two distributions (lower panel, blue) is used to determine peak position and width by fitting a Gaussian distribution.

the peak and thus could alter the peak shape. This was corrected by monitoring the measured rate of a fixed-frequency pulser.

For the required energy, the correct charge state had to be chosen. The charge state distribution at energies at the terminal of the tandem accelerator is lower than after the gas target at higher energy. However, because we did also measurements without gas in the gas target ('zero-pressure runs'), we had to pick a charge state that is sufficiently populated in both distributions. We selected a high charge state at the terminal, which is then on the low side of the distribution after the gas cell. E.g. at the 0.51 MeV/u we picked charge state 5+, which means the terminal voltage is 2.4 MV. The mean charge state at the terminal at this energy is 2.7 whereas after the gas target it is 6.6. This leads to a considerably intensity loss. Since we measure straggling only at one less populated charge state, the results might be biased. However, no systematic differences at the energies overlapping with JYFL were observed given the experimental error bars.

Because of the lower energy and the smaller apertures, the angular acceptance is small (0.5 mrad) compared to the JYFL setup with 3 mrad acceptance. As a consequence collisions with small impact parameters leading to large scattering angles are not measured. The effect is most pronounced for the Kr target. However, the critical impact parameter is smaller than the radius of the M shell for all cases except for Kr at low energies (< 2 MeV/u) and thus at our energies the effect is negligible.

2.2. K130 cyclotron at the Accelerator Lab JYFL

Measurements in JYFL were performed with a magnetically analyzed incident beam from the K130 cyclotron at energies of 1 to 12 MeV/u, covered in two beam times in 2014 (JYFL experiment A84) and 2015 (JYFL experiment A86), respectively. The energy profile of the ions after the gas cell is measured by the time-of-flight (TOF) technique (Fig. 3) similar to our previous experiment (JYFL experiment A75) with Kr beam [9]. Because of the higher energy the pressure in the 241 mm long gas cell needed to be higher (up to 1000 mbar) for sufficient energy loss, and therefore used thin 200 nm silicon nitride membranes[3] as entrance and exit windows. The gas pressure was measured by a piezoelectric manometer with 1% absolute accuracy.

The TOF measurements were based on three thin-film timepickoff detectors of the Busch et al. type [10], one start and two stop detectors at a distance of 2.139 m and 2.356 m, respectively. Electrons produced in thin carbon foils with a thickness of 10 μg/cm^2 are deflected onto a Multi-Channel Plate (MCP) detector to produce a fast timing signal. These two TOF measurements check for consistency, the Si-detector at the end provides an additional energy signal. The time resolution of both TOF measurements is around 100 ps. TOF spectra were accumulated to reach about 10^6 counts in the peak to minimize uncertainties from peak fitting. Note, the TOF measurements make no selection on the charge state and thus the measured data are from the entire charge state distribution.

Since energy changes at the cyclotron facility required substantial beam time, Al-degrader foils of several thicknesses ranging from 10 to 40 μm were occasionally inserted before two bending magnets to reduce the beam energy in small steps. However, in those runs with the energy degrader the energy distribution of the primary beam (measured without gas in the cell) was slightly higher. Thus in the data analysis we observed higher scatter of the measured straggling data that might be related on how the beam was tuned through the last bending magnet and the gas cell.

3. Data analysis

In both experiments the energy-loss profile was measured in He, N_2, Ne, Ar and Kr gases at several gas pressures. Additional measurements were performed without gas to see the primary energy distribution of the beam and in case of JYFL the effect of the silicon nitride windows. Those 'zero-pressure runs' were also used to calibrate the detectors and to determine the effective radius of the magnet at the ETH Zurich setup. The measured momentum spectra (ETH Zurich) and TOF spectra (JYFL), respectively, were converted into energy spectra. An example is shown in Fig. 4.

[3] made by Silson Ltd, http://silson.com

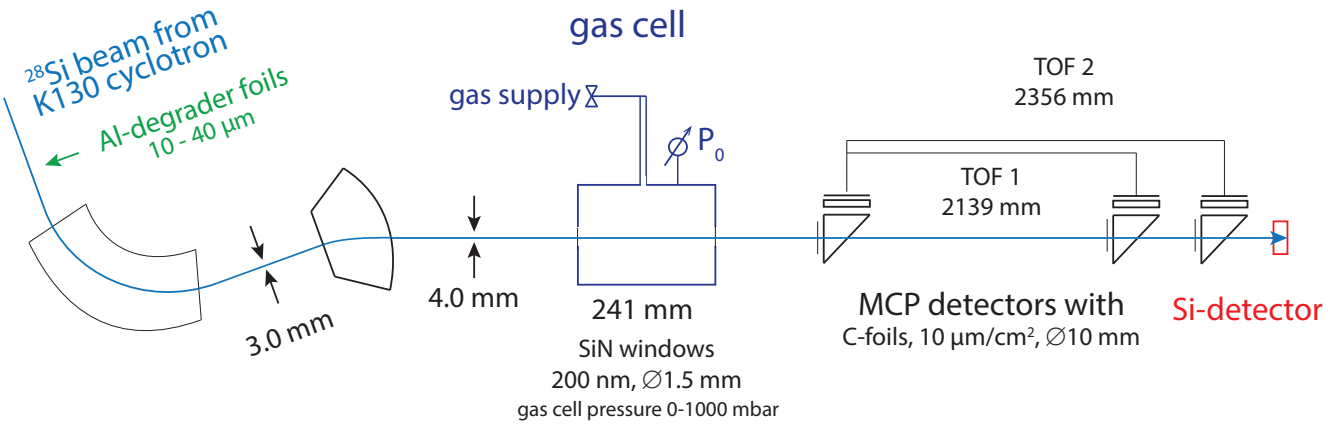

Figure 3: Experimental setup at K130 cyclotron at the Accelerator Lab JYFL.

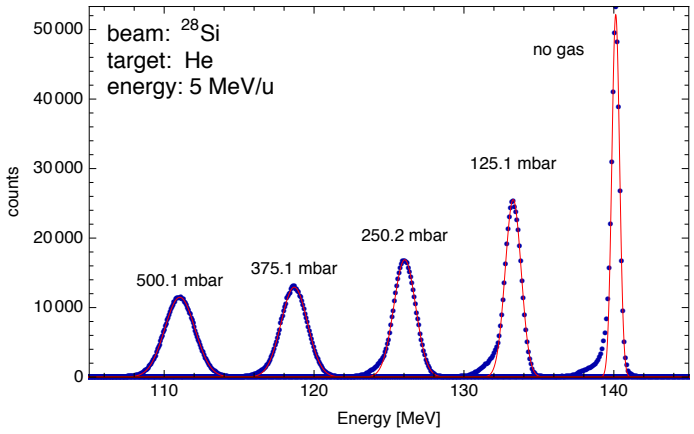

Figure 4: Superposition of measurements of ^{28}Si at 5 MeV/u at several He gas pressures and without gas. The red curves are Gaussian distributions fitted to the data. Measurements were performed at JYFL.

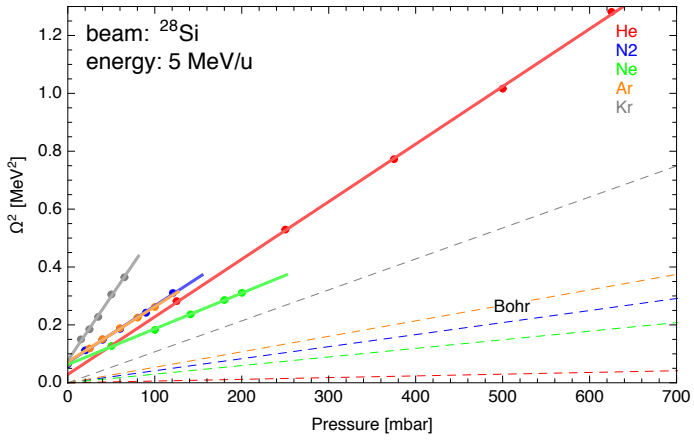

Figure 5: Ω^2 vs gas pressure of measurements of ^{28}Si at 5 MeV/u in several gases. The solid lines are linear fits to the measured data; the dashed lines are the expected slope from Bohr straggling. The width of 'zero-pressure' runs is not subtracted, thus the offset of the fits represents the width from beam energy spread, measurement resolution and straggling in the gas cell windows. Measurements were performed at JYFL.

As discussed in more detail in Ref. [9] we fitted a Gaussian shape to the energy profile; the shift of the centroid between the 'zero-pressure run' and the one with gas in the cell is used to calculate the mean energy loss; straggling was calculated from the FWHM of the fitted profile. Ω^2 is expected to be proportional to the target thickness and therefore, plotting the square of the width against target thickness is a test on the validity of the approximation (Fig. 5). The ratio of the slope of the linear fit to the data over the slope expected for Bohr straggling gives the ratio $\Omega^2/\Omega^2_{\mathrm{Bohr}}$. Because we determine the straggling ratio only from the slope we did not subtract the measurements without gas (measurements at zero pressure). The width of the zero-pressure measurements include initial beam energy spread, measurement resolution and effects of the entrance windows (at JYFL). We assumed that these contributions are independent of the pressure in the gas cell and thus it simply introduces an offset in the relation Ω^2 vs. target thickness.

At the ETH Zurich setup the effective target thickness was determined by the energy loss of the Si ions using the stopping power of SRIM-2013 [12]. This was compared to the value obtained from the central pressure and integrating over the pressure profile along the beam path, which agreed within 20%. At the JYFL the target thickness was calculated from the absolute pressure measurement, the target length and the temperature of 300 K. This allowed us furthermore to determine the stopping cross sections.

Experimental uncertainties were derived from the Gaussian fits and the linear regression to determine the slope. A minimal uncertainty of $\Omega^2/\Omega^2_{\mathrm{Bohr}}$ of 5% was assumed. Since the energy degrader runs at JYFL showed larger scatter we increased the error bar of $\Omega^2/\Omega^2_{\mathrm{Bohr}}$ at those energies by a factor of 2 to account for that scatter. Likewise a minimal error of 5% was assumed for the stopping cross section S.

4. Results and discussion

4.1. Stopping cross sections

The stopping cross sections S were extracted from the measurements at JYFL from the difference of the peak positions between the runs at different pressures in the gas cell. The target thickness was directly determined from the gas pressure. A comparison of the experimental data with the curve of the empirical interpolation code SRIM-2013 [12] and the PASS code [11] is shown in Fig. 6 and in Table 1.

In general the agreement between data of the two beam times and SRIM-2013 is very good except for the data of He and Kr at the lowest energy (1.16 MeV/u; see Fig. 6). Also the prediction by the standard PASS code (with Hartree-Fock atomic wave functions used for calculating shell corrections) agrees very well above $2-3$ MeV/u for gases N_2, Ne, Ar and Kr. In He gas the direct PASS output significantly underestimates the stopping cross section, however if double excitation and ionization [13] is included, the agreement is excellent. The effect of double ionization and excitation is, however, very small for the other gases as it decreases rapidly with target atomic number [13].

Without further measurements it is not clear whether the lower measured values at the lowest energy for He and Kr (Fig. 6) are an artefact of measurement with the energy degrader or the peak of the curve is less pronounced than SRIM-2013 predicts.

4.2. Energy-loss straggling

Figures 7 show our experimental results for the energy-loss straggling of Si in He, N_2, Ne, Ar and Kr gases. The recent theoretical calculations by Sigmund et al. [5] are also shown together with the empirical interpolation formula of Yang et al. [8]. The data are also summarized in Table 1.

The system Si–He (Figures 7) shows a pronounced peak around $4-5$ MeV/u. The width ($3-7$ MeV/u) and the amplitude ($\Omega^2/\Omega^2_{\mathrm{Bohr}} \sim 40$) is similar to the calculated peak by Sigmund et al. [5] with a peak position at 3 MeV/u, in contrast to the curve according to Yang et al. [8] which exhibits a broader maximum. Overlap of the data taken at ETH Zurich and JYFL at $1-2$ MeV/u shows an excellent agreement within experimental uncertainties between the two measurement setups. There is also good agreement of data at the peak ($4-5$ MeV/u) between different measurement times at JYFL. Larger scatter in the data is observed at higher energies (around 10 MeV/u) where the straggling enhancement is less and thus more difficult to measure precisely with the current setup. The theoretical curve by Sigmund et al. [5] shows an increase below 1 MeV/u towards lower energies which is not supported by our data (although there is only a single data point in this energy region). Clearly, more data in that energy region would help to clarify the situation.

The other systems investigated (Si in N_2, Ne, Ar and Kr) show a relatively flat energy dependence in the straggling, which again agrees qualitatively better with the curves calculated by Sigmund et al. [5] than with Yang et al. [8]. In general the straggling enhancement with a maximal $\Omega^2/\Omega^2_{\mathrm{Bohr}} \sim 5$ is weaker than for the system Si–He. There is some scatter in the experimental data that is beyond the error bars of the individual data points. Measurements done with the energy degrader (open symbols in Fig. 7) tend to result in higher $\Omega^2/\Omega^2_{\mathrm{Bohr}}$ values compared to measurements done with direct beam. Those values should be taken with caution and might represent an upper limit. Thus the current measurements can neither confirm nor exclude the weak structure seen in the straggling curves (Si in N_2, Ne, Ar and Kr) by Sigmund et al. [5].

5. Conclusions

We measured energy loss and straggling of Si ions in gases in the energy range of $0.5-12$ MeV/u. For the first time, a sharp energy-loss straggling peak could be measured in the system Si–He that was predicted by recent theoretical calculations by Sigmund et al. [5]. The strong and narrow enhancement over Bohr straggling is different from the shape of the Yang straggling [8] and a direct consequence of charge-exchange straggling. In the other investigated gases (N_2, Ne, Ar and Kr) a much weaker energy dependence was found which is in good agreement with the new theoretical calculations that show such a weak structure. This structure could not be resolved with the current uncertainties of the measurement. In order to demonstrate the predicted multi-peak structure in the energy-loss straggling either higher measurement precision is needed (which is difficult to achieve with the current setup) or one has to look for another beam-target combination that shows a pronounced peak similar to Si–He [7].

Acknowledgement

This work is a direct outcome of a close collaboration of the authors with Peter Sigmund (University of Southern Denmark, Odense, Denmark) and Andreas Schinner (Johannes Kepler University, Linz-Auhof, Austria); their primary motivation, theoretical input and valuable discussions have been essential for these experiments. We acknowledge the support by the EU 7th framework programme Integrating Activities - Transnational Access, by the Academy of Finland under the Finnish Centre of Excellence Programme 2012-2017.

[1] N. Bohr, Philos. Mag. **30** (1915) 581
[2] F. Besenbacher, J. U. Andersen, and E. Bonderup, Nucl. Instrum. Methods **168** (1980) 1
[3] P. Sigmund and A. Schinner, Europ. Phys. J. D **58** (2010) 105
[4] P. Sigmund, O. Osmani, A. Schinner, Nucl. Instrum. Methods B **269** (2011) 804
[5] P. Sigmund, O. Osmani and A. Schinner, Nucl. Instrum. Methods B **338** (2014) 101
[6] P. Sigmund, *Particle penetration and radiation effects volume 2* (Springer Series in Solid State Sciences, vol. 179, Springer, Heidelberg, 2014)
[7] P. Sigmund and A. Schinner, Nucl. Instrum. Methods B **384** (2016) 30
[8] Q. Yang, D. J. O'Connor and Z. Wang, Nucl. Instrum. Methods B **61** (1991) 149
[9] C. Vockenhuber, J. Jensen, J. Julin, H. Kettunen, M. Laitinen, M. Rossi, T. Sajavaara, O. Osmani, A. Schinner, P. Sigmund, H. J. Whitlow, Eur. Phys. J. D **67** (2013) 145
[10] F. Busch, W. Pfeffer, B. Kohlmeyer, D. Schull, F. Puhlhoffer, Nucl. Instrum. Methods **171** (1980) 71
[11] P. Sigmund, A. Schinner, Nucl. Instrum. Methods B **195** (2002) 64

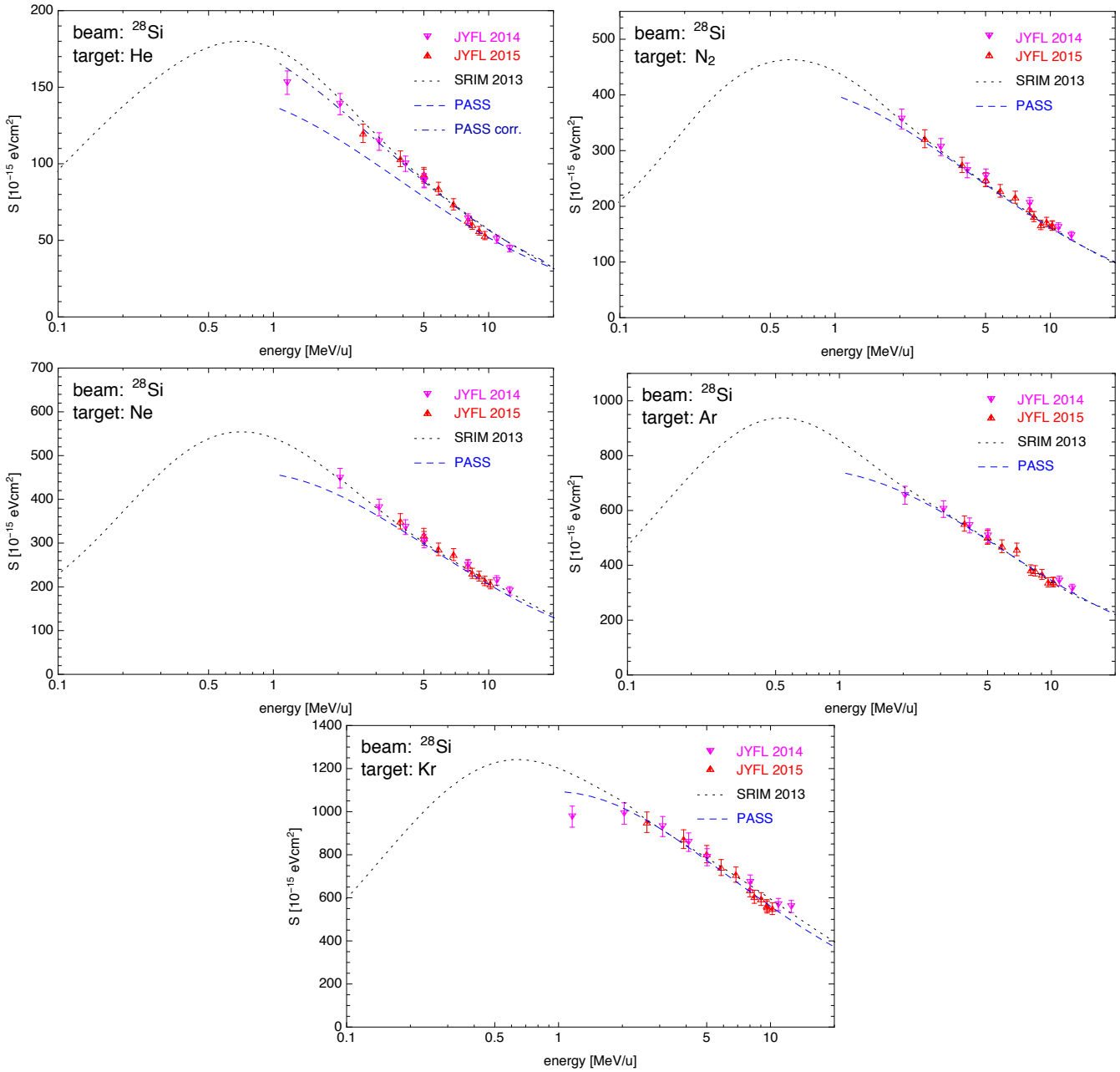

Figure 6: Stopping cross sections for Si in in He, N_2, Ne, Ar and Kr gases. Present measurements (from JYFL) are compared to data from SRIM [12] and PASS [11]. For He gas the corrected PASS curve is also shown that includes double excitation and ionization [13].

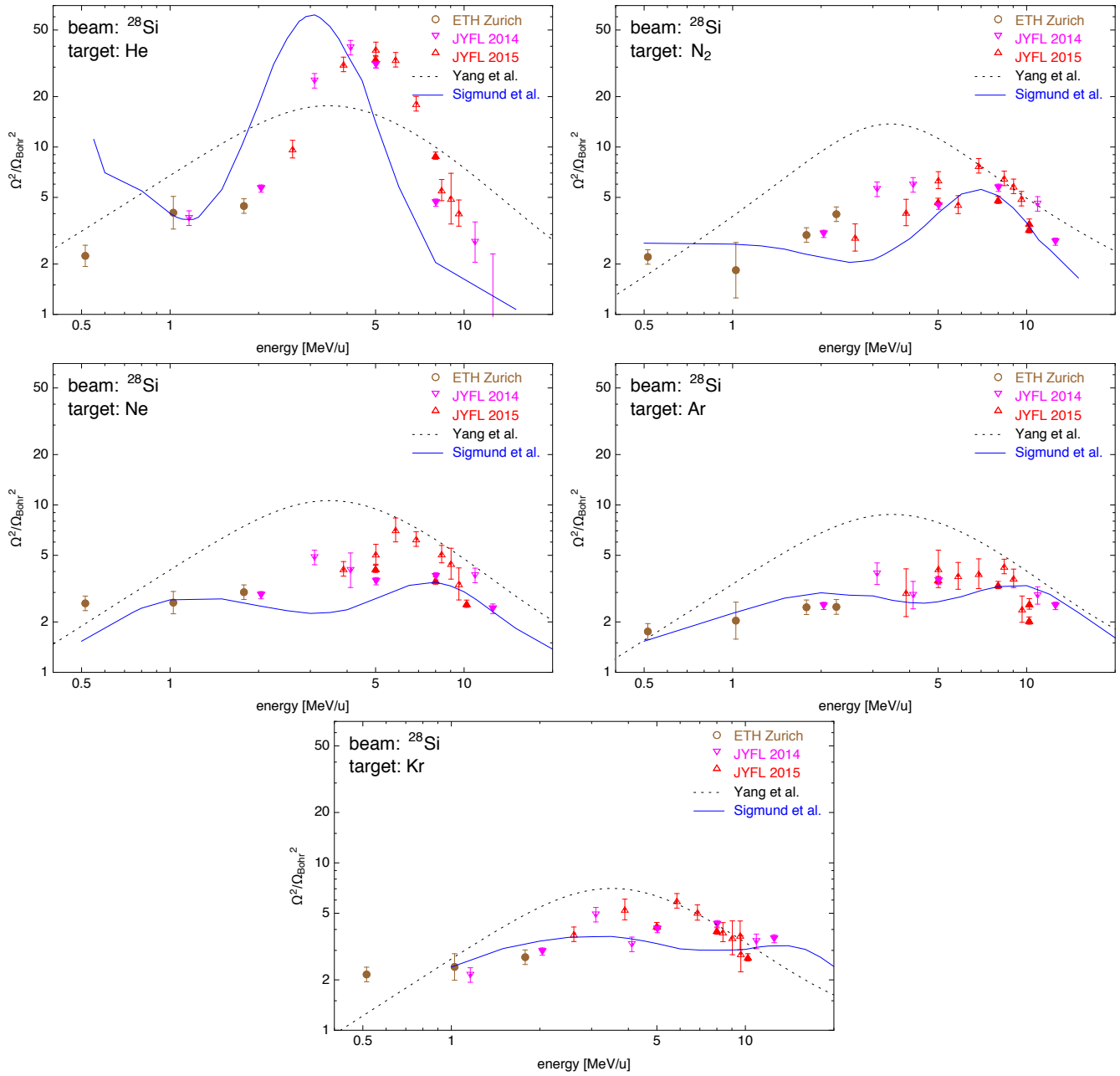

Figure 7: Straggling of Si relativ to Bohr straggling in He, N_2, Ne, Ar and Kr gases. Measured data are shown with different symbols according to measurement location and beam time. Open symbols of the JYFL data indicate measurements with energy-degraded beam that yield larger scatter or increased error bars. The empirical interpolation formula of Yang et al. [8] is shown as dotted line; the solid line denotes the theoretical curves by Sigmund et al. [5].

[12] J.F. Ziegler, Particle interactions with matter (2012), www.srim.org
[13] P. Sigmund, private communication (2016)

Table 1: Summary of measured stopping cross sections S and straggling ratios $\Omega^2/\Omega^2_{\mathrm{Bohr}}$ grouped according to experiment and beam time. Energies marked with a star (*) are taken with energy degrader. Note, not all target-energy combinations were measured because of technical or time restrictions.

	Si-He		Si-N_2		Si-Ne		Si-Ar		Si-Kr	
Energy (MeV/u)	S (10^{-15} eVcm^2)	$\Omega^2/\Omega^2_{\mathrm{Bohr}}$	S (10^{-15} eVcm^2)	$\Omega^2/\Omega^2_{\mathrm{Bohr}}$	S (10^{-15} eVcm^2)	$\Omega^2/\Omega^2_{\mathrm{Bohr}}$	S (10^{-15} eVcm^2)	$\Omega^2/\Omega^2_{\mathrm{Bohr}}$	S (10^{-15} eVcm^2)	$\Omega^2/\Omega^2_{\mathrm{Bohr}}$
				ETH Zurich						
0.51		2.23 ± 0.3		2.20 ± 0.2		2.58 ± 0.2		1.75 ± 0.1		2.15 ± 0.2
1.03		4.04 ± 0.9		1.83 ± 0.7		2.60 ± 0.4		2.03 ± 0.5		2.38 ± 0.4
1.78		4.43 ± 0.4		2.97 ± 0.2		3.01 ± 0.3		2.44 ± 0.2		2.73 ± 0.2
2.25				3.96 ± 0.3				2.45 ± 0.2		
				Experiment A84 – JYFL 2014						
1.16 *	152 ± 7	3.75 ± 0.3							976 ± 48	2.13 ± 0.2
2.04	138 ± 6	5.64 ± 0.2	356 ± 17	3.02 ± 0.1	448 ± 22	2.88 ± 0.1	655 ± 32	2.49 ± 0.1	991 ± 49	2.95 ± 0.1
3.10 *	114 ± 5	24.8 ± 2.4	306 ± 15	5.59 ± 0.5	381 ± 19	4.85 ± 0.4	604 ± 30	3.88 ± 0.5	930 ± 46	4.90 ± 0.4
4.11 *	100 ± 5	39.2 ± 3.9	264 ± 13	5.93 ± 0.5	336 ± 16	4.07 ± 0.9	545 ± 27	2.89 ± 0.5	858 ± 42	3.25 ± 0.3
5.01	89 ± 4	31.2 ± 1.5								
5.02	88 ± 4	31.1 ± 1.5	254 ± 12	4.45 ± 0.2	304 ± 15	3.50 ± 0.1	507 ± 25	3.53 ± 0.1	788 ± 39	4.02 ± 0.2
8.02	64 ± 3	4.65 ± 0.2	205 ± 10	5.70 ± 0.2	249 ± 12	3.74 ± 0.1			672 ± 33	4.29 ± 0.2
10.90 *	50 ± 2	2.70 ± 0.7	162 ± 8	4.57 ± 0.4	214 ± 10	3.79 ± 0.3	343 ± 17	2.87 ± 0.3	568 ± 28	3.39 ± 0.3
12.53	44 ± 2	0.68 ± 0.8	147 ± 7	2.72 ± 0.1	190 ± 9	2.39 ± 0.1	315 ± 15	2.49 ± 0.1	559 ± 27	3.52 ± 0.1
				Experiment A86 – JYFL 2015						
2.61 *	119 ± 5	9.71 ± 1.1	321 ± 16	2.88 ± 0.5					951 ± 47	3.74 ± 0.3
3.89 *	103 ± 5	31.1 ± 3.1	274 ± 13	4.06 ± 0.7	349 ± 17	4.15 ± 0.4	552 ± 27	2.98 ± 0.9	872 ± 43	5.26 ± 0.7
5.00	93 ± 4	33.4 ± 1.6	247 ± 12	4.70 ± 0.2	317 ± 15	4.15 ± 0.2	501 ± 25	3.55 ± 0.1	802 ± 40	4.18 ± 0.2
5.01 *	91 ± 4	38.2 ± 3.8	247 ± 12	6.33 ± 0.7	310 ± 15	5.07 ± 0.6	503 ± 25	4.15 ± 1.0	740 ± 37	5.93 ± 0.5
5.85 *	83 ± 4	33.2 ± 3.3	227 ± 11	4.52 ± 0.5	285 ± 14	7.09 ± 1.1	469 ± 23	3.76 ± 0.6	707 ± 35	5.05 ± 0.5
6.87 *	73 ± 3	18.1 ± 1.8	216 ± 10	7.72 ± 0.7	273 ± 13	6.25 ± 0.6	457 ± 22	3.88 ± 0.7	636 ± 31	3.93 ± 0.1
8.00	62 ± 3	8.87 ± 0.4	195 ± 9	4.83 ± 0.2	248 ± 12	3.53 ± 0.1	382 ± 19	3.32 ± 0.1	604 ± 30	3.85 ± 0.5
8.39 *	60 ± 3	5.52 ± 0.8	181 ± 9	6.49 ± 0.6	230 ± 11	5.08 ± 0.6	379 ± 18	4.28 ± 0.4	594 ± 29	3.56 ± 0.8
9.03 *	56 ± 2	4.91 ± 1.7	166 ± 8	5.81 ± 0.5	224 ± 11	4.45 ± 0.9	366 ± 18	3.64 ± 0.4	563 ± 28	3.68 ± 0.7
9.60 *	53 ± 2	4.02 ± 0.7	171 ± 8	4.91 ± 0.4	213 ± 10	3.37 ± 0.7	337 ± 16	2.38 ± 0.4	557 ± 27	2.85 ± 0.7
10.20			165 ± 8	3.22 ± 0.1	205 ± 10	2.56 ± 0.1	339 ± 16	2.03 ± 0.1	549 ± 27	2.72 ± 0.1
10.21			165 ± 8	3.49 ± 0.2			338 ± 16	2.56 ± 0.1		